Journal of Sound and Vibration (1998) **214**(5), 903–913
Article No. sv981577

ANALYTICAL AND EXPERIMENTAL MODAL ANALYSIS FOR OPERATIONAL VALIDATION AND CALIBRATION OF A MINIATURE SILICON SENSOR

P. Q. Zhang*, X. L. Tang, B. X. Shan

Department of Modern Mechanics, University of Science and Technology of China, Anhui, Hefei 230026, *People's Republic of China*

AND

J. A. Brandon and A. S. K. Kwan

*Cardiff School of Engineering, University of Wales Cardiff, Cardiff, CF*2 3*TB, Wales*

(*Received* 18 *December* 1997, *and in final form* 24 *February* 1998)

The development of micromechanical sensors poses new challenges in design, calibration and operation. The paper reports a study where analytical and experimental techniques are applied to a prototype sensor. Analytically, a substructuring method is used together with a proprietary finite element package. Experimentally, novel excitation and response transducers are used to provide input data for specialised time domain identification algorithms. The resulting comparisons provide confidence in the combination of techniques used in the study.

1. INTRODUCTION

The advent of micro-mechanical systems has posed new challenges, not only in the operational use of the devices but also in their calibration. In the current study, a micro-machined sample was tested with the primary objective being to gain experience in techniques of calibration and insights into the variability and stability of the operational characteristics of such sensors.

The present study provides an opportunity to evaluate the effectiveness of a number of techniques which have to be validated in context. For example output-only modal identification algorithms almost invariably have an implicit assumption about the spectral characteristics of the input. This type of assumption can be assessed only in the context of a particular test design. A key assumption in the present study, for example, is that the spectrum generated by the novel spark–pulse excitation was uniform white noise.

2. THE PRINCIPLE OF THE RESONATING BEAM FORCE SENSOR (RBFS)

The principle of the resonating beam force sensor (RBFS) is that the force to be measured is used to induce changes in the boundary conditions of a beam [1, 2]. The specific sensor used in this study is illustrated in Figure 1. This results in changes in its frequency response properties which are sensed by inducing, and observing, a resonant condition. The device has a simple structure and uniform properties. In principle, the sensing of the applied force can then be attained with an analog control system. Integration

* Professor Zhang is currently Visiting Professor in the Cardiff School of Engineering.

0022–460X/98/300903 + 11 $30.00/0

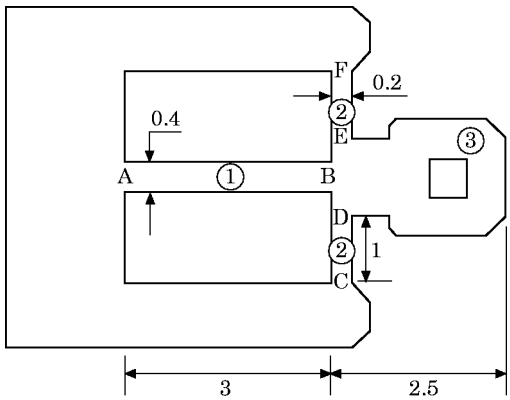

Figure 1. Geometry of the resonating beam force sensor. ① Resonant beam; ② transverse beam; ③ force-imposed ring. Dimensions in mm.

into a microcomputer based control system is straightforward. In designing such a sensor there are several key design considerations [3, 4]. Firstly, the no-load natural frequencies of the device should be determined. The characteristics of the material should ensure sharp resonance characteristics—high dynamic amplification and narrow frequency spread. The geometry of the sensor should be optimized to minimise power flow out of the resonating beam. The modal characteristics should be identified so as to determine the appropriate excitation and response measurement points.

In assessing the effectiveness of a design, predictability of operational performance, stability of response and repeatability in manufacture are of primary concern. The project involved the analysis and testing of 30 devices to assess these parameters.

The miniature silicon resonating beam force sensor is shown in Figure 1. It comprises one resonating beam (AB, 3 mm $\times$ 0·4 mm), two transverse beams (CD and FE, 1 mm $\times$ 0·2 mm) and a force transmission ring. When a tensile axial force N (see Figure 2) acts on the ring the natural frequencies will be shifted correspondingly. Thus, subject to a reliable calibration, the axial force can be determined based on the frequency shift.

The excitation element and vibration detection element are all integrated in a resonating beam made of silicon. The output signal of a detection element is exported to a selective frequency amplifier, and is fed back to the excitation element, which constitutes a positive-feedback self-oscillation system. The operational resonance frequencies as a function of the axial force can be converted into digital signals in order to estimate the axial force N as shown in Figure 2.

A key design criterion for this class of sensors is that the modes should be well spaced, particularly where coupling of bending and torsional vibrations is possible.

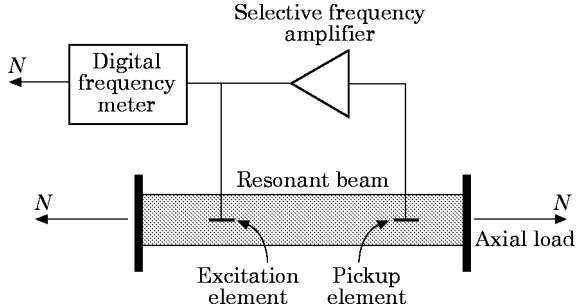

Figure 2. Operational principle of the resonating beam force sensor.

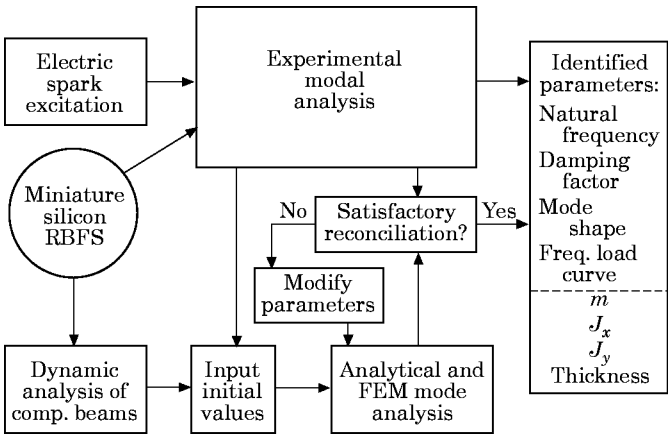

Figure 3. Schematic layout of the mode correlation and model adjustment.

3. DYNAMIC PARAMETER IDENTIFICATION OF THE SILICON RBFS

Because of the fabrication technique employed, the width and length of the sensor can be accurately controlled whereas the thickness of the beam is difficult to control. These variations in thickness have a substantial effect on the operational natural frequencies and damping of the resonating beam element.

The use of non-contacting actuators and sensors is essential in this context. For example, attachment of actuators may cause ambiguities in analysing the excitation conditions [4], whereas the mass of a sensor will materially affect the dynamics of the structure. In the present study an optical transducer system, the Working Point Locking Michelson Interferometer (WPL-MI), was employed.

Because of the fragility of the specimen, an excitation system combining broadband spectral properties with low energy input optimised the balance between information requirements and risk of damage. The technique chosen was the Pulse Electric Spark exciter. A voltage of 6 kV causes a spark lasting a few microseconds. The resulting shock wave fulfils the desired excitation conditions, exciting the lower order natural frequencies of the beam.

Multi-point excitation was achieved by using multiple electrodes, in this case three, deployed according to prior knowledge of the mode shapes from the theoretical analysis. From the results of these two methods, not only are the first six modal parameters estimated, but the thickness of the beams, the mass and the rotational mass moment of inertia of the force transmission ring are also determined. The block diagram of this identification process is shown in Figure 3.

3.1. ANALYTICAL PREDICTION OF RESPONSE CHARACTERISTICS

The geometry of the sensor (see Figure 1) is sufficiently regular to allow the use of a sub-structuring method. In essence, the sensor was approximated by using several simple beam elements and a rigid body element. The formation of the local equations and the subsequent assembly of the substructures is described in Appendix 1. The assembled structure results in a low order eigenvalue problem which produces estimates of the mode shapes and natural frequencies of the sensor. These are shown in Table 1.

The validity of this approach was supported by results from a proprietary finite element package†. The results are given in table 1. Mode shapes are illustrated in Figure 4.

† The package used was SAP5.

TABLE 1

Representative measured, predicted and estimated properties

	Experimental modal analysis						
	MS-STRM		MCRM		FEM	Substructure analysis	
Mode number	Freq. (kHz)	Damping factor	Freq. (kHz)	Damping factor	Frequencies (kHz)	Freq. (kHz)	Characteristic of the mode
1	2·461	0·030	–	–	2·311	2·456	Global
2	11·14	0·006	11·24	0·002	12·17	11·13	Vibration
3	16·85	0·036	16·95	0·002	15·92	16·90	Torsional vibration of the resonating beam (RB)
4	–	–	–	–	24·68	–	Global vibration in the plane xOy
5	39·65	0·003	39·70	0·002	34·72	39·56	Bending vibration of the resonating beam (RB)
6	105·7	0·007	105·8	0·010	–	107·8	
7	214·7	0·004	211·8	0·001	–	211·7	

Other estimated parameters: $J_x = 0{\cdot}71$ mg mm^2, $J_x = 4{\cdot}50$ mg mm^2; thickness of the resonating beam, 45·8 μm; mass of the force ring, 1·340 mg. Independently measured parameters: thickness of the resonating beam (by laser), 45·0 μm; mass of the force ring (by analyzer), 1·33 mg.

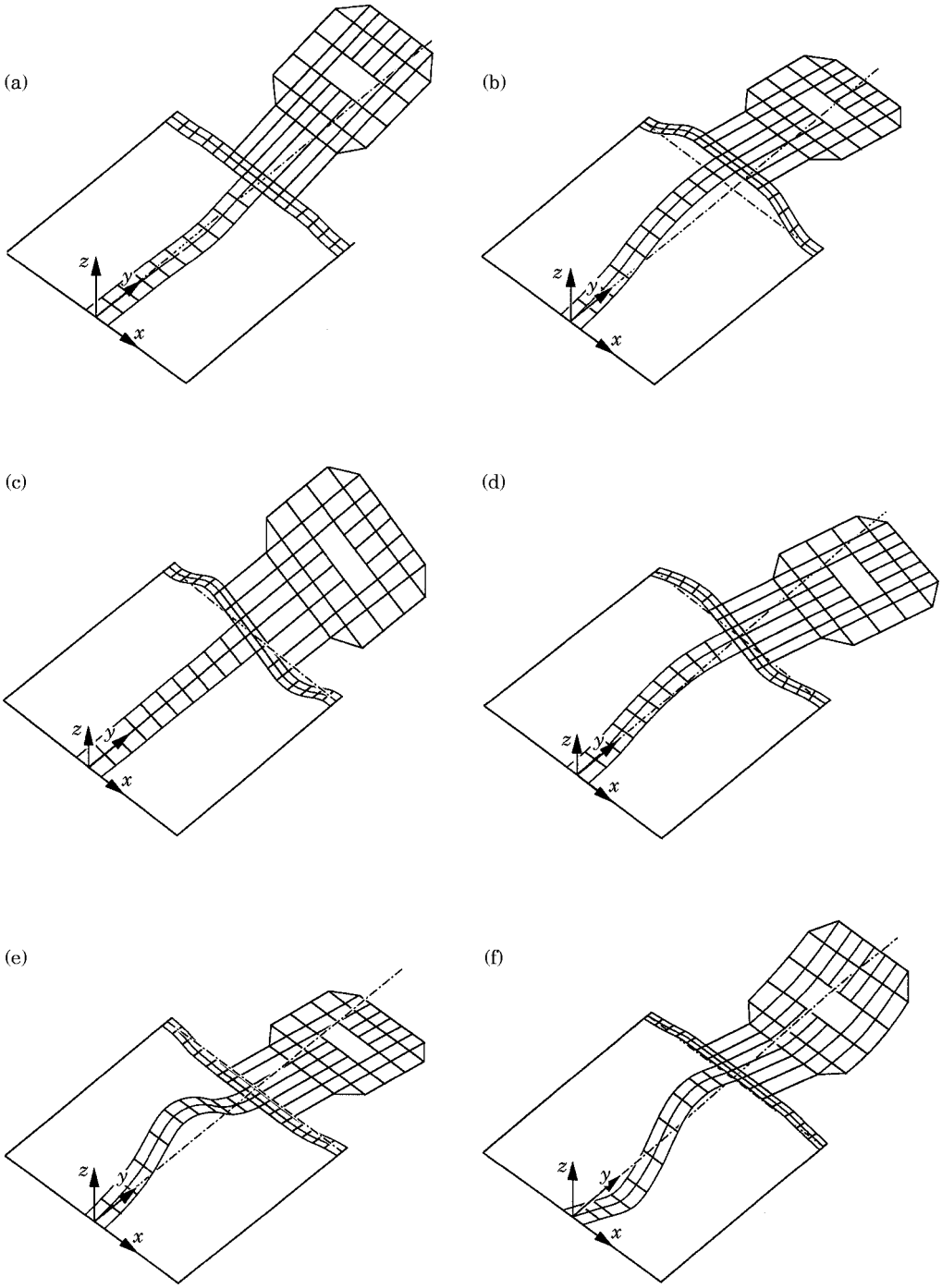

Figure 4. Computed mode shapes. Mode number, frequency (kHz): (a) 1, 2·31; (b) 2, 12·17; (c) 3, 15·92; (d) 4, 24·68; (e) 5, 34·72; (f) 6, 78·2.

As has already been described, the in-plane dimensions of micromechanical sensors are much easier to control during the etching process than the thickness of the sensor. The measured response properties were used to provide estimates of the sensor thickness which was then used in the analytical models.

3.2. EXPERIMENTAL RESULTS

As has been described, modal identification techniques which rely on measurements of outputs only require an implicit assumption of the excitation spectrum [5]. In the present study two different time domain modal parameter identification methods were used. The first, Multiple Single-Input Space-Time Regressive Method [6], uses a classical autoregressive modelling approach. (See, for example, reference [7]). The second, the Modal Correlation Recurrence Method [8], uses a more specialized correlation model based on the modes of the system. In each method the natural frequencies and damping factors of each mode are estimated.

3.3. MODE CORRELATION AND MODEL ADJUSTMENT

The results presented in Table 1 were computed as the result of an iterative model refinement procedure. The information flow of the model adjustment process is shown in Figure 3. As will be described, the extreme localization of the high frequency modes effectively allowed the reference beam to be modelled as a clamped-clamped beam. This enabled the initial estimation of the geometric and inertia parameters (thickness, m, J_x, J_y). Other modes contribute further information. For example, the moment of inertia of the force ring about the y-axis dominates the kinetic energy of the third mode.

The estimated thickness of the sensor was referred to an independent measurement by using a laser diffraction sensor. The estimate of mass was compared with an independent value obtained by using a precision weighing instrument. These data provided a basis for the scaling of the properties presented in Table 1.

4. DISCUSSION

As has been described, there are several criteria for choice of a reference mode for the RBFS. For example: the energy to excite the mode should be as small as practicable (implying, in turn, low power flows to the surrounding structures and low modal damping), the variation of frequency with applied load should be stable, repeatable and, ideally, linear, the mode should have a condition at, or close to, an antinode at both the excitation and measurement points.

From the identified modes (see Table 1 and Figure 4), it is clear that the first two mode shapes have a number of undesirable features. The modes are global modes with amplitudes which are higher outside the reference beam than they are internally. Mode 2, particularly, has a high amplitude for the force ring.

The third mode has a significant displacement within the reference beam but this is primarily torsional and will not be reliably detectable by the interferometer. In addition, this mode is insensitive to changes in the applied load—rendering it useless for the estimation of the applied load. As has been remarked, the fourth mode is entirely in-plane and was, consequently, not measured in the experimental modal surveys.

The fifth, sixth and seventh modes all have response characteristics localized to the reference beam. The beam is behaving essentially as a clamped–clamped beam. Thus each of these modes satisfies the criterion of localization of the modal energy.

With increasing frequency the repeatability of the modal identification degraded. In general, a high degree of repeatability was observed for the fifth mode whereas the

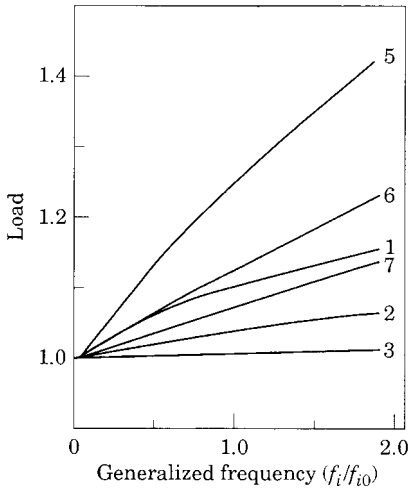

Figure 5. Load-frequency sensitivity. f_i is ith resonance frequency; f_i, is ith natural frequency.

estimation of the response properties of the sixth and seventh modes proved unreliable. As can be seen from Figure 5, linearity of the frequency load characteristic curves is satisfactory for each of these modes although the sensitivity of the fifth mode, once again, is advantageous.

When the mode shape is considered the fifth mode confirms its preferability. In contrast to, particularly, the sixth mode the beam is antinodal in precisely the region where accessibility for excitation and response is best.

The seventh mode (not illustrated) is the logical successor to the fifth and sixth, having its modal response localized within the reference beam span but with two nodes within the span. In comparison to the fifth mode the internodal span is significantly shorter limiting the accessibility of instrumentation. The resonance frequency (typically 200 kHz) was approximately five times as high as for the fifth mode (typically 40 kHz) with

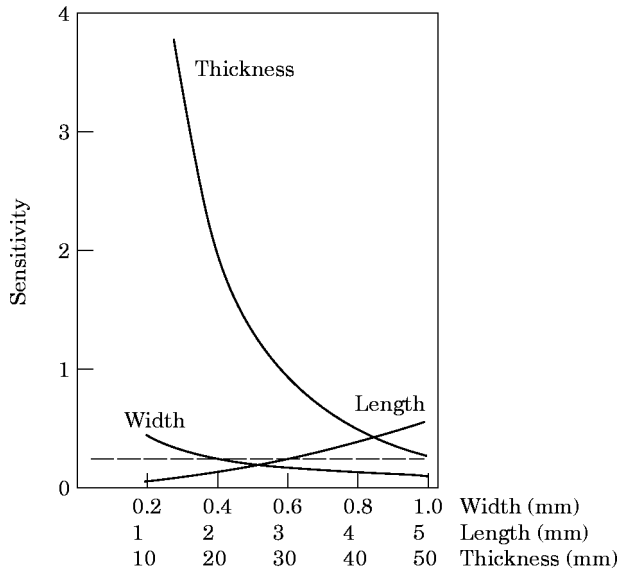

Figure 6. Dimension sensitivity of the fifth mode.

implications for reduced amplitude for equivalent modal energy. This mode also was less satisfactory in terms of stability, repeatability and linearity—defined earlier as key criteria.

With the focus now on the fifth mode, a sensitivity analysis is illustrated in Figure 6. In this analysis the thickness varies from 13 μm to 46 μm, the width from 0·2 mm to 1 mm, and the length from 1 mm to 5 mm. It is apparent that the thickness of the sensor is the key variable. For example, when the thickness of the resonating beam is decreased from 46 μm to 13 μm, the width and the length do not change, the relative sensitivity will increase from 0·23 to 3·73: i.e., when the sensor is loaded to 1 N, the resonance frequency will be approximately 3·73 times as great as the unloaded case. However it should be kept in mind that the mechanical robustness of the sensor may be compromised if it is made too thin. Increasing strength by increasing the width of the sensor will not compromise its sensitivity.

5. CONCLUSION

This paper has described an investigation of the applicability of a number of methods, which are proven for use for macroscopic structures, on a micromechanical sensor. The methods used provide a consistent basis for structural testing of micromechanical devices. Because of the wide variety of devices and test methods the success of the identification process for this class of sensors does not automatically extend to other classes of devices.

The study has provided useful design information which will lead to refinement of the characteristics of the experimental prototype sensor.

ACKNOWLEDGMENTS

This work was supported by the National Natural Science Foundation of China and the Cardiff Advanced Chinese Engineering Centre of the University of Wales, Cardiff.

REFERENCES

1. F. R. Blom, S. Bouwstra, J. H. J. Fluitman and M. Elwenspoek 1989 *Sensors and Actuators* **17**, 513–519. Resonating silicon beam force sensor.
2. H. A. C. Tilmans, M. Elwenspoek and J. H. J. Fluitman 1992 *Sensors and Actuators A* **30**, 35–53. Micro resonant force gauges.
3. P. Q. Zhang, X. L. Tang, Q. M. Wang and T. C. Huang 1992 *Proceedings of the* 10*th International Modal Analysis Conference*, *San Diego*, 683–687. Experimental modal analysis of a miniature resonating beam force sensor.
4. J. A. Brandon and H. G. D. Goyder 1989 in *Modern Practice in Stress and Vibration Analysis* (Editor J. Mottershead) Oxford: Pergamon Press, 59–67. A strategy for quality assurance in theoretical and experimental modal analysis.
5. C. F. Cremona and J. A. Brandon 1992 *Proceedings of the American Society of Civil Engineers*, *Journal of Aerospace Technology* **5**, 442–449. Modal identification algorithm with unmeasured input.
6. T. C. Huang, P. Q. Zhang and W. Q. Feng 1986 *International Journal of Analytical and Experimental Modal Analysis* **1**, 1–7. Multiple single-input space time regression method in modal analysis.
7. L. Ljung 1987 *System Identification*: *Theory for the User*. Englewood Cliffs, NJ: Prentice-Hall.
8. Q. J. Yang 1991 *Ph.D. Dissertation*, *University of Science and Technology of China*, *Hefei*. Experimental modal analysis theory and parameter identification of general linear vibration systems.
9. R. R. Craig Jr. 1981 *Structural Dynamics*: *An Introduction to Computer Methods*. New York: John Wiley.

APPENDIX 1: DETAILS OF SUBSTRUCTURING METHOD

Considering the resonating beam element shown in Figure A1, under axial load N, couples M, and lateral end loads F, one can express the differential equation of the bending vibration [9] as

$$EI\frac{\partial^4 V(y,t)}{\partial y^4} - N\frac{\partial^2 V(y,t)}{\partial y^2} + \rho A\frac{\partial^2 V(y,t)}{\partial t^2} = 0 \tag{A1}$$

and the differential equation of the torsional vibration as

$$I_p\,\partial^2\theta(y,t)/\partial t^2 = KGJ\,\partial^2\theta(y,t)/\partial y^2. \tag{A2}$$

Here $V(y,t)$ is the dynamic transverse deflection, and $\theta(y,t)$ is the angle of twist along the beam (y is the co-ordinate position along the member and t is time). EI is the bending stiffness, ρA is the density of the beam in mass per unit length, GJ is the torsional stiffness, I_p is the polar mass moment of inertia per unit length, and K is the shape factor which is purely dependent on the geometry of the beam cross-section.

After an extensive mathematical reduction, one can obtain the dynamic stiffness matrices in terms of a consistent beam theory under an axial load:

$$\begin{bmatrix} F_A \\ F_B \\ M_A \\ M_B \\ T_A \\ T_B \end{bmatrix} = \begin{bmatrix} K_B & 0 \\ 0 & K_T \end{bmatrix} \begin{bmatrix} V_A \\ V_B \\ \phi_A \\ \phi_B \\ \theta_A \\ \theta_B \end{bmatrix}. \tag{A3}$$

Here F_A, F_B, M_A, M_B, T_A, T_B are the shear forces, bending moments and torques at each end of the beam respectively, and V_A, V_B, ϕ_A, ϕ_B, θ_A, θ_B are the bending deflections, bending slopes, and torsional angles at each end of the beam respectively. K_B (4×4) and K_T (2×2) are the bending and torsional dynamic stiffness matrices respectively, both of which are dependent on material, inertia and geometric parameters of the beam.

The resonating beam is fixed to the frame at one end, and connected to the force transmission ring at the other. Considering that the stiffness of the ring is much larger than

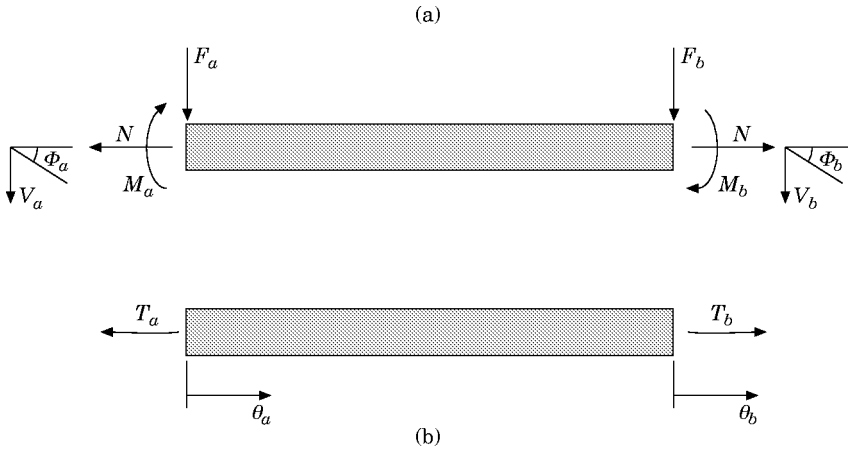

Figure A1. Substructure model for beam element.

that of either the resonating, or transverse, beam, one can safely regard the ring as a rigid body. One thus has the following boundary conditions:
(a) clamped conditions,

$$V_A = V_C = V_F = 0, \qquad \phi_A = \phi_C = \phi_F = 0, \qquad \theta_A = \theta_C = \theta_F = 0; \tag{A4}$$

(b) deflection continuity conditions,

$$\theta_B = -\phi_D = -\phi_E = \theta, \qquad \phi_B = \theta_D = \theta_E = \phi, \qquad V_B = V, \qquad V_D = V + (\Delta/2)\theta,$$
$$V_E = V - (\Delta/2)\theta. \tag{A5}$$

Here V is the lateral deflection of point B, θ is the torsional angle along the resonating beam at point B, ϕ is the bending slope at point B, and Δ is the width of the ring.

The equations of motion of the force transmission ring can be obtained as:

$$M_B + T_D + T_E = \omega^2(\phi J_x + m l_4 V),$$
$$M_D + M_E - T_B + (F_E - F_D)\Delta/2 = -\omega^2 \theta J_y,$$
$$F_B + F_D + F_E = m\omega^2(l_4\phi + V). \tag{A6}$$

Here m is the mass of the ring. J_x and J_y are the rotational mass moments of inertia of the ring around the axes of the transverse, and resonating, beam respectively, and l_4 is the distance between the centre of the mass of the ring and B.

The characteristic matrix of the whole structure, obtained by rearrangements of equations (A3)–(A6), takes the form

$$\begin{bmatrix} k_{11} & k_{12} & 0 \\ k_{21} & k_{22} & 0 \\ 0 & 0 & k_{33} \end{bmatrix} \begin{bmatrix} V \\ \theta \\ \phi \end{bmatrix} = \{\mathbf{0}\} \tag{A7}$$

The non-trivial solution for $[V\ \theta\ \phi]^{\mathrm{T}}$ is obtained from equating the determinant of the matrix to zero:

$$k_{33} = 0, \qquad \text{or} \qquad k_{11}k_{22} - k_{12}k_{21} = 0. \tag{A8, A9}$$

Equation (A8), relating to the torsional vibration modes of the resonating beam, and equation (A9) to the bending modes, are called the characteristic equations. They are the implicit analytic functions of the natural frequencies, the solutions of which give the natural frequencies of the sensor.

APPENDIX 2: INSTRUMENTATION AND EXPERIMENTAL PROCEDURES

To record the vibration signals, a Working Points-Locking Michelson Interferometer (WPL-MI) was used. A problem common to the traditional Michelson Interferometer is fringe instability. Generally speaking, low frequency fringe instability is caused by: thermal expansion of optical components, mechanical base vibration and fluctuating air currents, which obscure an inteferometric measurement. In such circumstances the use of working point stabilization systems provides more constant sensitivity. In Figure A2 it is shown that the integrated output signal of the photoelectric multiplier tube (PMT) of a Michelson interferometer is fed back to the reference mirror controlled by an acoustic transducer. This constitutes a servo control system where the working point is locked in. From a typical frequency response function of the WPL-WI, it is observed that when a frequency is much less than f_c (f_c is the resonance frequency of WPL-MI), the response of WPL-MI

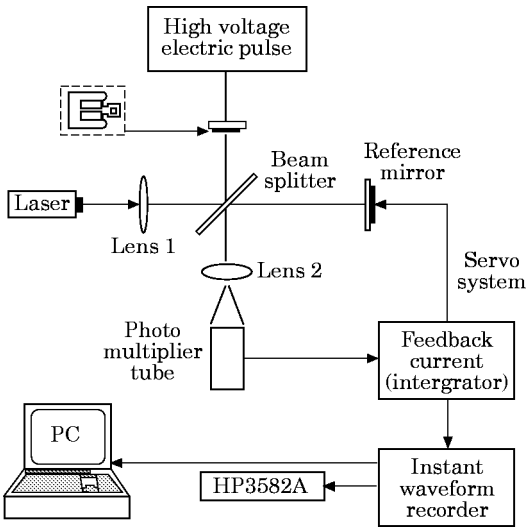

Figure A2. Schematic diagram of the instrumentation.

tends to be zero: i.e., the reference mirror has compensated the low frequency noise successfully. On the other hand, when the device (sensor beam) is vibrating at a higher frequency ($>f_c$), the response of WPL-MI effectively has a constant sensitivity. Thus the WPL-MI acts like a high-pass filter. The resolution of WPL-MI is about 1–5 nm. So due to its high sensitivity and stability, the WPL-MI has been used successfully to measure the free response time history of the sensor beam under the PES excitation.